RESEARCH ARTICLE

Characterization and estimation of human airway deposition of size-resolved particulate-bound trace elements during a recent haze episode in Southeast Asia

Sailesh N. Behera · Raghu Betha · Xian Huang · Rajasekhar Balasubramanian

Abstract Toxic elements present in airborne particulate matter (PM) are associated with human health effects; however, their toxic characteristics depend on the source of their origins and their concentrations in ambient air. Twenty four elements (Al, B, Ba, Be, Bi, Ca, Cd, Co, Cr, Cu, Fe, Ga, K, Li, Mg, Mn, Na, Ni, Pb, Se, Sr, Te, Tl, and Zn) in 12 different size fractions of PM ranging from 10 nm to 10 μm were characterized in Singapore during two different atmospheric conditions (smoke haze and non-haze periods) in 2012 for the first time. In addition, their possible sources were identified based on backward air trajectory analysis and principal component analysis (PCA). The health implications of inhalable particles were assessed using a human airway deposition model, the Multiple-Path Particle Dosimetry model (MPPD). The results concerning particle-bound trace elements are interpreted in terms of coarse ($PM_{2.5-10}$), fine ($PM_{2.5}$), ultrafine ($PM_{0.01-0.1}$, 0.01 μm$<$Dp$<$0.10 μm), and nano ($PM_{0.01-0.056}$, 0.01 μm$<$Dp$<$0.056 μm) particles. The ratios of elemental concentrations measured between the smoke haze episode and the non-haze period in coarse, fine, ultrafine, and nano particles varied from 1.2 (Bi) to 6.6 (Co). Both the PCA and backward trajectory analysis revealed that trans-boundary biomass-burning emissions from Indonesia were primarily responsible for enhanced concentrations of particulate-bound elements during the smoke haze episode. The particle depositions in the respiratory system were higher during the smoke haze episode compared to the non-haze period. The study finds that ultrafine and nano particles present in the atmosphere have higher tendencies to be deposited into the deeper parts of the respiratory system, compared to coarse and fine particles.

Keywords Smoke haze · Biomass burning · Respiratory deposition · Size-resolved PM · Toxic elements · Principal component analysis

S. N. Behera · R. Betha · X. Huang · R. Balasubramanian (✉)
Department of Civil and Environmental Engineering, National University of Singapore, Singapore 117576, Republic of Singapore
e-mail: ceerbala@nus.edu.sg

Introduction

Particulate matter (PM) is a mixture of chemical constituents that have both natural and anthropogenic origins (Fang et al. 2005; Behera and Sharma 2010; Khare and Baruah 2010). Among the constituents of PM, some trace elements are potentially toxic in nature. For example, even in lower concentrations, particulate-bound Cd, Cr, Cu, Fe, Mn, Ni, Pb, and Zn can cause harmful health effects among exposed individuals on a short-term and/or long-term basis depending on many factors, including their inherent toxicity, concentrations, time, duration, and place of exposure. Toxicity studies in the past confirmed that elements associated with ambient PM catalyze the formation of reactive oxygen species (ROS), leading to oxidative stress, and the production and release of inflammatory mediators by the respiratory tract epithelium (Carter et al. 1997; Ghio et al. 1999; Wilson et al. 2002; Mura'nszky et al. 2011).

In the past, several studies characterized trace elements in fine particles ($PM_{2.5}$; PM with aerodynamic diameter (AED) ≤2.5 μm) and coarse particles ($PM_{2.5-10}$) in different urban environments (Kim et al. 2003; Koulouri et al. 2008; Clements et al. 2014). Recent studies indicated that ultrafine ($PM_{0.1}$) and nano ($PM_{0.05}$) particles play a major role in triggering a series of health problems, including premature death, aggravated asthma, and chronic bronchitis, due to their ability to penetrate easily into the alveolar region of the lungs

(Asgharian and Price 2007; Martins et al. 2010; Sioutas et al. 2005; Russell and Brunekreef 2009; Leiva et al. 2013; Farina et al. 2013). Therefore, it is essential to characterize size-resolved particulate elements (specifically ultrafine and nano particles) and assess their potential health effects through its deposition mechanisms inside the human body.

The frequent occurrence of forest and peatland fires in Indonesia due to land-clearing activities releases large amounts of PM with unique chemical compositions into the atmosphere (Balasubramanian et al. 2003; Abas et al. 2004; Hyer and Chew 2010; See et al. 2006, 2007; Betha et al. 2013; Reid et al. 2013). The resultant particulate emissions undergo trans-boundary transportation, and are transformed into regional smoke haze episodes affecting several neighboring countries in Southeast Asia (SEA), most notably Singapore, Malaysia, Indonesia, and Thailand (Heil and Goldammer 2001; Reid et al. 2013). The frequent occurrence of biomass-induced smoke haze episodes in SEA during dry seasons with elevated PM levels is a matter of public health concern in view of a high population density situated in this region (Balasubramanian et al. 1999, 2003). Smoke haze episodes also occur in other parts of the world, such as China, India, USA, and South America, and have therefore received considerable attention because of their impacts on atmospheric visibility, cloud formation, and even global climate (e.g., Menon et al. 2002; Nel 2005; Tan et al. 2009).

The size of PM is an important factor to consider for health impact assessments because AEDs determine where each particle is likely to be deposited in the human respiratory system upon inhalation (Herner et al. 2006; Ham et al. 2010). In the past, several studies (e.g., Nazaroff et al. 1993; Venkataraman and Raymond 1998; Alfoldy et al. 2009) have used particulate size distribution data to estimate respiratory deposition efficiencies, based on laboratory-scale experiments. Szoke et al. (2007) used ambient size-resolved composition data obtained through field experiments to estimate respiratory deposition efficiencies. Ham et al. (2010) studied the patterns of respiratory deposition efficiencies of health-relevant trace elements in size-distributed PM during a severe winter in California's San Joaquin Valley, USA. Subsequently, Ham et al. (2011) carried out a more extensive study to estimate respiratory deposition efficiencies with respect to size-distributed PM in different seasons. However, systematic studies on size-resolved elemental characterizations of PM and their associated human health risks are lacking during smoke haze episodes.

During the past decades, several studies were conducted to investigate the potential environmental and health impacts of smoke haze episodes through physicochemical and toxicological characterization of PM in tropical urban environments situated in SEA (e.g., Balasubramanian et al. 2003; Abas et al. 2004; See et al. 2007; Hyer and Chew 2010; Pavagadhi et al. 2013). In all the previous studies, the

emphasis was placed on the characterization of particles that were PM$_{2.5}$ or bigger, during biomass burning-induced smoke haze episodes. However, the chemical characterization and health impacts of smaller particles (ultrafine and nano particles) remain poorly understood. In this study, we characterized 24 elements (Al, B, Ba, Be, Bi, Ca, Cd, Co, Cr, Cu, Fe, Ga, K, Li, Mg, Mn, Na, Ni, Pb, Se, Sr, Te, Tl, and Zn) in different size fractions of PM, ranging from 10 nm to 10 μm, during two different atmospheric conditions (smoke haze and non-haze periods) in a tropical urban atmosphere (Singapore: latitude 1° 17′ N and longitude 103° 50′ E; Fig. 1) within SEA from September to November 2012. The possible sources of these elements were identified on the basis of principal component analysis (PCA) analysis. The measured concentrations of all trace elements were used in a human airway deposition model, Multiple-Path Particle Dosimetry model (MPPD), to estimate deposition patterns within each region of the human respiratory system (i.e., head, tracheobronchial, and pulmonary) in order to identify suitable mitigation measures for the purpose of protecting public health.

Methodology and experiments

Sampling site

This field study was conducted at the Atmospheric Research Centre (67 m above the sea level and about 1 km from the open sea), National University of Singapore (NUS), located at the southern tip of the Malayan Peninsula, between latitudes 1° 09′ N and 1° 29′ N and longitudes 103° 36′ E and 104° 25′ E (Fig. 1). The important sources of PM pollution in Singapore are combustion activities occurring in industries, including oil refineries and power plants, transportation through vehicles, and domestic cooking (Behera et al. 2013). Apart from these emission sources, Singapore faces an increase in PM levels when trans-boundary smoke resulting from forest and peatland fires in Indonesia reach Singapore and transformed into a smoke haze episode. From past records, it has been observed that smoke haze episodes occur largely from May to October, when uncontrolled forest and peat fires take place in Indonesia, and the southwest monsoon prevails in the region (Balasubramanian et al. 2003; See et al. 2007; Betha et al. 2014; Behera and Balasubramanian 2014).

Sampling campaign

Size-segregated PM samples were collected by using micro-orifice uniform deposition impactor (MOUDI) (model 100R, MSP Corp, USA) and nanomicro-orifice uniform deposition impactor (NanoMOUDI) (model 115, MSP Corp, USA) samplers. The collection of PM samples was done in different size ranges, 5.6–10, 3.2–5.6, 1.8–3.2, 1.0–1.8, 0.56–1.0, 0.32–0.56,
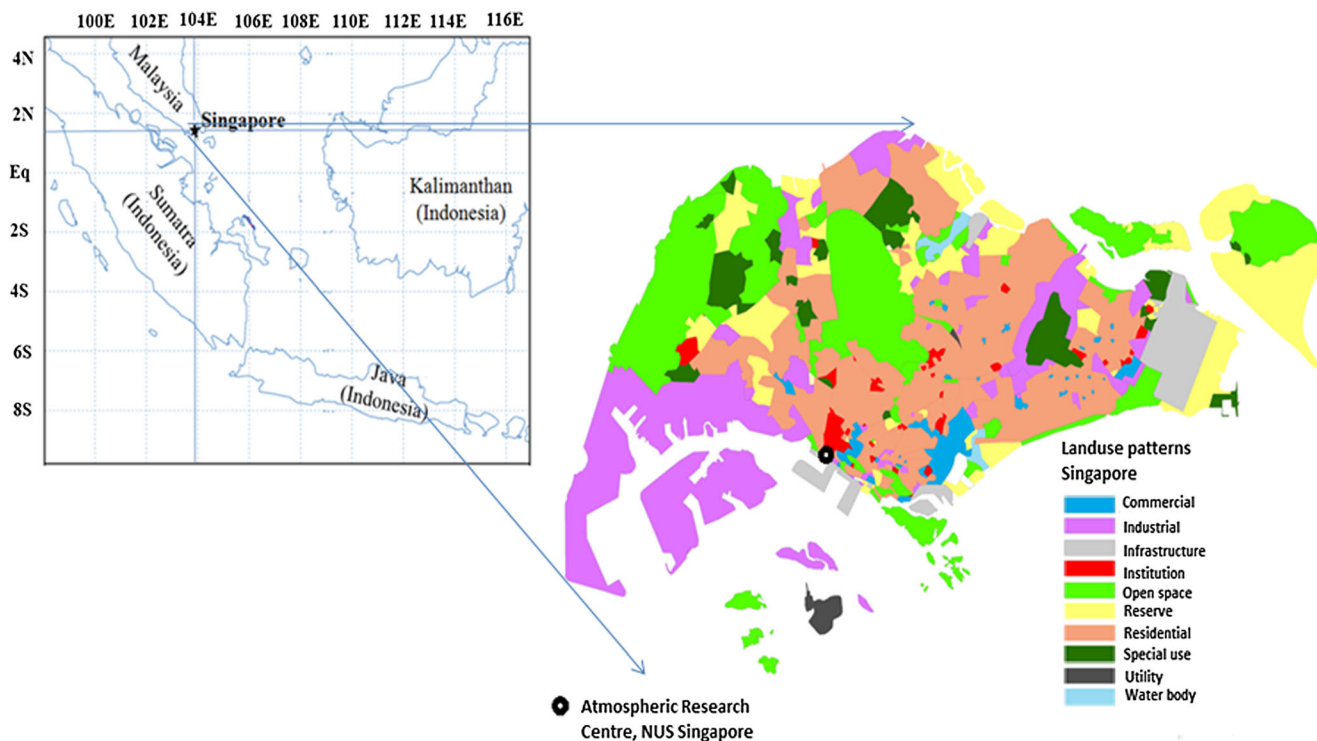
Fig. 1 A map showing the study area Singapore and its neighboring regions in Southeast Asia and the location of the Atmospheric Research Centre (sampling site) at NUS, Singapore

0.18–0.32, 0.10–0.18, 0.056–0.100, 0.032–0.056, 0.018–0.032, and 0.010–0.018 μm. In this study, the experimental data is reported in terms of four size groups: coarse ($PM_{2.5–10}$), fine ($PM_{2.5}$), ultrafine ($PM_{0.01–0.1}$, 0.01 μm<D_p<0.10 μm), and nano ($PM_{0.01–0.056}$, 0.01 μm<D_p<0.056 μm) particles.

Ambient air was drawn at air flow rates of 30 liters per minute (LPM) and 10 LPM, respectively, for MOUDI and NanoMOUDI samplers. The impactor plates were loaded with preconditioned (T=22 °C and relative humidity (RH)=35 %) and pre-weighed (Microbalance; Sartorius, MC 5) polytetrafluoroethylene (PTFE) filters (Pall Corporation, USA). Post-sampling conditioning and weighing of the exposed filters were performed, using methods that were similar to pre-sampling filters. PM mass concentrations in different size ranges were estimated by dividing the mass of the particles collected on filters by the volume of air sampled. The duration of air sampling was 48 h. During this measurement campaign, four and five sets of smoke haze and non-haze samples were collected, respectively. Altogether, a total of 108 PM samples were collected for gravimetric and chemical analyses. During the sampling program, meteorological parameters (temperature, RH, wind speed, wind direction, and rainfall) were acquired every 5 min by an automated meteorological station located at the sampling site. Temperature and RH were measured using suitable sensors (Vaisala, model CS500), while wind speed and wind direction were measured using an anemometer and a wind vane (RM Young, model 03001). The entire system was connected to a Console/

Receiver (Part Number 6310) and to a personal computer via WeatherLink for Vantage Pro data logger (CSI, model CR10X). Table 1 shows the period of the sampling program, meteorological parameters (temperature, RH), and pollution indicators (pollution standard index (PSI), $PM_{2.5}$) during the field campaign.

Elemental characterization

Our established protocol for the analysis of total particulate elements was used in this study (Karthikeyan et al. 2006). The method is summarized here. In this method, 4 mL of HNO_3, 2 mL of H_2O_2, and 0.4 mL of HF are put into a Teflon vessel along with half of the sampled filter or blank filter. Samples in the Teflon vessels undergo digestion through a closed vessel microwave digestion system (MLS-1200 mega, Milestone Inc., Italy), after the vessels are capped. In this study, the digestion process was performed at three stages of power requirements; i.e., 250 W for 5 min, followed by 400 W for 5 min, and finally, 600 W for 2 min. After completing the digestion processes, all relevant sample extracts were filtered carefully through 0.2-μm Teflon membrane filters and diluted to 50 mL with ultra-pure water (Millipore). The filtered samples meant for the analysis of total elements in the instrument of inductively coupled plasma mass spectrometry (ICP-MS) were refrigerated at 4 °C for further analysis. For quality control procedures on recovery tests, we prepared samples of SRM 1648a for the analysis of total elements.

Table 1 Details of sampling program conducted during 2012

Sample set no	Period of sampling	Temp (°C)	RH (%)	WS (m/s)	WD (°)	RF (mm)	PSI[a]	PM$_{2.5}$ (μg/m^3)[a]
During smoke haze episode								
1	16/9/2012 to 17/9/2012	28.5	76.8	2.3	202	0.0	59	56
2	20/9/2012 to 21/9/2012	27.9	74.8	2.2	198	0.0	64	63
3	30/9/2012 to 1/10/2012	28.2	75.3	1.9	192	0.0	56	54
4	8/10/2012 to 9/10/2012	27.5	78.9	2.4	205	0.0	53	51
During non-haze period								
1	3/10/2012 to 4/10/2012	28.4	80.6	2.1	125	0.1	26	24
2	29/10/2012 to 30/10/2012	28.6	77.5	3.2	86	0.0	28	27
3	31/10/2012 to 1/11/2012	27.6	70.5	1.8	87	0.0	17	16
4	3/11/2012 to 4/11/2012	25.8	79.5	2.1	131	0.1	22	21
5	6/11/2012 to 7/11/2012	26.1	76.4	1.8	65	0	18	16

Temp temperature, *RH* relative humidity, *WS* wind speed, *WD* wind direction, *RF* rainfall, *PSI* pollution standard index

[a] The data were taken from NEA, Singapore

The instrument ICP-MS (Agilent 7700 Series, USA) was used for analyses of total elements present in the extracted samples. During the sample run, it was observed that the flow rates of the plasma gas, auxiliary gas, and nebulizer gas were observed to be 15, 1, and 1 LPM, respectively. Filtered samples were introduced at a rate of 1 mL/min, and waste removal was conducted from the nebulizer through a peristaltic pump.

We collected field blanks of 47-mm PTFE filters at regular intervals. These blank filters were subjected to the same storage, handling, and analytical protocols as field samples for both MOUDI and NanoMOUDI impactors. The limit of detection (LOD) of any species of an analytical method depends only on the capability of the instrumental system. On the other hand, the method detection limit (MDL) accounts for various uncertainties that occur during sampling, extraction, calibration, matrix effect, recovery, etc. Therefore, there are significant differences between LOD and MDL of a specific method. In this study, we estimated both LOD and MDL of each element for two different sampling conditions (MOUDI and NanoMOUDI impactors) as per the procedures reported in the literature (e.g., Dillner et al. 2007; Homazava et al. 2008; Kabir et al. 2011; Kim and Kim 2012).

The MDL of each element was estimated based on the product of standard deviation of seven replicates of the filter blank values multiplied by the Student's *t* value at 99.9 % confidence level (USEPA 1991), as shown in Eq. (1):

$$MDL = t \times S \tag{1}$$

where *t*=Student's *t* value for a 99 % confidence level with *n*−1 degrees of freedom (*t*=3.14 for seven replicates) and *S*= standard deviation of the replicate analyses.

The LOD of each element was determined as three times the standard deviation of background noise of seven replicates

of filter blank values. Table 2 presents the estimated LOD and MDL of each element in two different sampling systems, expressed in the unit of nanogram per cubic meter. It is to be noted that the measured ambient concentration levels of each element were higher than the respective LOD values.

The validity of the system calibration as part of quality control/quality assurance protocol was performed by using spiked samples after every 10 samples. We used an exact amount of 10 mg SRM 1648a for total element recovery studies. We estimated the analytical recovery of target elements by comparing the results of total elements from the extracted samples with certified values for SRM 1648a. Equation (2) shows the estimation method for recovery as

$$\% \text{ recovery} = \frac{\text{Concentration obtained from extracted samples}}{\text{Concentration from certified values}} \times 100 \tag{2}$$

The recovery of total elements fell in the range of 92–108 %. These values are within the acceptable range recommended by the Association of Analytical Communities. In the ICP-MS, a seven-point calibration was performed with concentrations of 2, 5, 10, 20, 50, 75, and 100 μg/L of standards for each batch of analysis. In all calibration plots, it was observed that the regression coefficients for all 24 elements were more than 0.999.

Principal component analysis

To further identify the possible sources for particulate-bound elements in the atmosphere, the PCA method was used, as

Table 2 Limits of detection (LODs) and method detection limits (MDLs) for elements analyzed in this study under two different sampling conditions

Elements	LOD (ng/m³)[a]	MDL (ng/m³)[b]	LOD (ng/m³)[c]	MDL (ng/m³)[d]
Al	0.181	0.422	0.073	0.151
B	0.092	0.167	0.039	0.065
Ba	0.141	0.247	0.061	0.088
Be	0.001	0.002	0.001	0.001
Bi	0.001	0.002	0.001	0.001
Ca	0.205	0.585	0.076	0.218
Cd	0.001	0.002	0.001	0.001
Co	0.009	0.012	0.005	0.006
Cr	0.056	0.118	0.022	0.044
Cu	0.097	0.224	0.036	0.079
Fe	0.210	0.446	0.088	0.156
Ga	0.019	0.042	0.016	0.027
K	0.135	0.328	0.113	0.146
Li	0.009	0.011	0.003	0.005
Mg	0.219	0.498	0.078	0.172
Mn	0.075	0.111	0.030	0.045
Na	0.146	0.326	0.050	0.131
Ni	0.132	0.274	0.050	0.098
Pb	0.023	0.045	0.009	0.018
Se	0.127	0.224	0.045	0.080
Sr	0.019	0.031	0.008	0.012
Te	0.011	0.014	0.004	0.006
Tl	0.007	0.009	0.003	0.004
Zn	0.170	0.370	0.057	0.131

LOD of individual elements was estimated using three times the standard deviation of background noise of seven replicates. MDL of individual elements was estimated as the product of standard deviation of seven replicates multiplied by the Student's t value at 99.9 % confidence level, i.e., degree of freedom, $df=6$ and $t=3.14$

[a] LOD for the ICP-MS method with 47-mm field blank Teflon filter in NanoMOUDI impactor and sampling volume of 28.8 m³

[b] MDL for the ICP-MS method with 47-mm field blank Teflon filter in NanoMOUDI impactor and sampling volume of 28.8 m³

[c] LOD for the ICP-MS method with 47-mm field blank Teflon filter in MOUDI impactor and sampling volume of 86.4 m³

[d] MDL for the ICP-MS method with 47-mm field blank Teflon filter in MOUDI impactor and sampling volume of 86.4 m³

several studies reported its usefulness for source apportionment (Henry and Hidy 1979; Henry et al. 1984; Thurston and Spengler 1985; Carmine et al. 1999; Salvador et al. 2004; Vallius et al. 2008; Kothai et al. 2011). This method has been widely used to factorize the input concentration data of different species, assuming a linear relationship between the total mass concentration and the individual concentrations of different species. In this approach, several steps are involved for the mathematical method to group the elemental data. In the first step, the concentration data is converted into a dimensionless form by standardization, as shown in Eq. (3):

$$X_{it} = \frac{C_{it} - C_i}{d_i} \qquad (3)$$

where C_{it} is the concentration of the variable i in the sample t and C_i and d_i are the arithmetic mean and standard deviation of the variable i for all samples included in the analyses.

The PCA model is expressed as Eq. (4):

$$X_{it} = \sum_{j=1}^{N} L_{ij} S_{jt} + E_{it} \qquad (4)$$

where L_{ij} is the factor loading of the variable i in the source j with N number of sources, S_{jt} is the factor score of the source j for sample t, and E_{it} is the residual of variable i in the sample t not accounted by the j sources or factors. The PCA model (Eq. (3)) is solved by eigenvector decomposition. Then, a varimax normalized rotation is applied to maximize or minimize the values of the loading factors of each compound analyzed in relation to each rotated principal component, and this provides the most interpretable structure to the factors.

Deposition modeling in the respiratory system

The experimental results were used in a human airway deposition model (MPPD model, MPPD v 2.11; Asgharian and Anjilvel 1998) to estimate the deposition patterns within each region (head, tracheobronchial, and pulmonary) of the human respiratory system. The MPPD model was developed by the Chemical Industry Institute of Toxicology and the Dutch National Institute of Public Health and Environment to estimate human and rat airway particle dosimetry. The theoretical foundations of the MPPD model are described by Anjilvel and Asgharian (1995). The details of the model are described in Winter-Sorkina et al. (2002). Several papers reviewed the use and validation of the MPPD model applications (e.g., Teeguarden et al. 2007; Rostani et al. 2009). In the context of its application in aerosol characteristics, several research groups (Oberdorster et al. 2004; Elder and Oberdorster 2006; Nong et al. 2009; Kane et al. 2010; Ham et al. 2011) are using the model to estimate the patterns of deposition of various sizes of particulate chemical species in different regions of the human respiratory system.

In this study, the dosimetry modeling through the MPPD model was performed with certain assumptions, listed as follows: spherical particles with nose-only breathing, a tidal volume of 625 mL, and a breathing frequency of 12 breaths/

min to simulate the respiratory system of an average human adult.

Two important parameters of the size-distributed PM mass and particulate elemental mass are the mass median aerodynamic diameter (MMAD) and geometric standard deviation (GSD). We followed a log-probit method described by O'Shaughnessy and Raabe (2003) to estimate the MMAD and GSD values for each elemental species, based on data obtained from actual field measurements. With the assumptions mentioned above and the values of MMAD and GSD, size-resolved deposition fractions were estimated for each region of the respiratory tract (i.e., head, tracheobronchial, and pulmonary). The results from MPPD modeling for size-resolved deposition fractions were utilized to estimate the deposited mass of a chemical species in each size bin. In other words, the deposited mass of a chemical species in a specific size bin was estimated by multiplying the mass of a chemical species with a corresponding deposition fraction. Then, the deposited masses estimated in each size bin were summed up to an AED of 2.5 μm to find a combined fine particle deposition value. The specific deposition efficiency of each species in each respiratory tract was estimated as deposited, per microgram $PM_{2.5}$ mass inhaled during the smoke haze episode and the non-haze period.

Results and discussions

Overall results

Figure 2 shows the particle mass size distributions observed during the smoke haze episode and the non-haze period. The PM mass showed bimodal distributions during both these periods. During the smoke haze episode, the dominant mass peak occurred at 0.56–1.0 μm, followed by a secondary peak at 1.8–5.6 μm. On the other hand, during the non-haze period, the maximum mass peak occurred at 0.18–0.32 μm, followed by a secondary peak at 1.8–3.2 μm. The latter patterns of particle size distributions were also observed in some of the earlier studies conducted in different parts of the world (e.g., Venkataraman et al. (1999) in Mumbai, India; Tan et al. (2009) in Guangzhou, China). The particle size distribution observed during the smoke haze episode is similar to the one reported by Duan et al. (2006) in Guangzhou, China.

In addition to the above observations, the aerosol MMAD shifted towards a larger particle size (0.95 μm) during the smoke haze episode, compared to the one observed during the non-haze period (0.88 μm). We compare this observation to the study by Lai et al. (2009), in which they assessed the influence of smoke haze (caused by rice straw burning) on the size distribution of PM mass. Lai et al. (2009) observed that the mass median diameters (MMD) in the particulate phase

were 0.92 and 1.21 μm, during non-burning and burning periods, respectively, at one of the sites in Taiwan. Based on this observation, Lai et al. (2009) concluded that freshly emitted particles from rice straw burning probably undergo hygroscopic growth during their transport, resulting in a larger MMD, compared to those emitted from local urban sources.

A possible explanation in the context of observations in this study is that biomass burning emitted more fine particles than coarse particles, which were then transported to Singapore (See et al. 2006). During the long-range transport process, some finer particles agglomerated, resulting in an increase in the sizes of particles as well (See et al. 2006; Betha et al. 2013). With the help of scanning electron microscope (SEM) images during the smoke haze and the non-haze periods, See et al. (2006) concluded that the particles from local sources (non-haze) are freshly emitted and young in nature. On the other hand, particles associated with the smoke haze episode are aged in nature and formed through particle agglomeration.

PM in the size range from 0.4 to 1.0 μm is classified as accumulation mode particles, whereas PM in the size from 2.5 to 10.0 μm is referred to as coarse mode particles (Lin et al. 2005; Duan et al. 2012). In general, it is believed that PM in the accumulation mode is mainly responsible for light scattering due to their high scattering efficiency (See et al. 2006; Lai et al. 2009). It was observed that the total mass of the accumulation mode PM was close to that of the coarse mode PM during the non-haze period. However, the total mass PM in the accumulation mode PM was more than that of the coarse mode PM during the haze period, implying that biomass burning-induced smoke haze episodes might have a strong influence on regional climate change. These observations are consistent with those made for other biomass burning events in that PM in the accumulation mode is dominant during haze episodes (Yang et al. 2006; Karar and Gupta 2007; Lai et al. 2009).

The total mass of airborne particles classified in different size ranges (coarse, fine, ultrafine, and nano particles; see "Sampling campaign") was much higher during the smoke haze episode, in comparison to that within the non-haze period. Specifically, the mean concentrations of coarse, fine, ultrafine, and nano particles during the smoke haze episode were 2.7, 3.2, 1.5, and 1.6 times of the concentrations of the non-haze period, respectively. The relative enhancement in the mass of PM in the fine mode during the smoke haze episode could be due to freshly emitted particles or new particle formation in the accumulation mode (Fang et al. 2005; Zhang et al. 2010).

Elemental characterization

The elemental concentrations in all sizes of particles were higher during the smoke haze episode than those during the

Fig. 2 Levels of size-distributed PM during the (**a**) smoke haze episode and (**b**) non-haze period
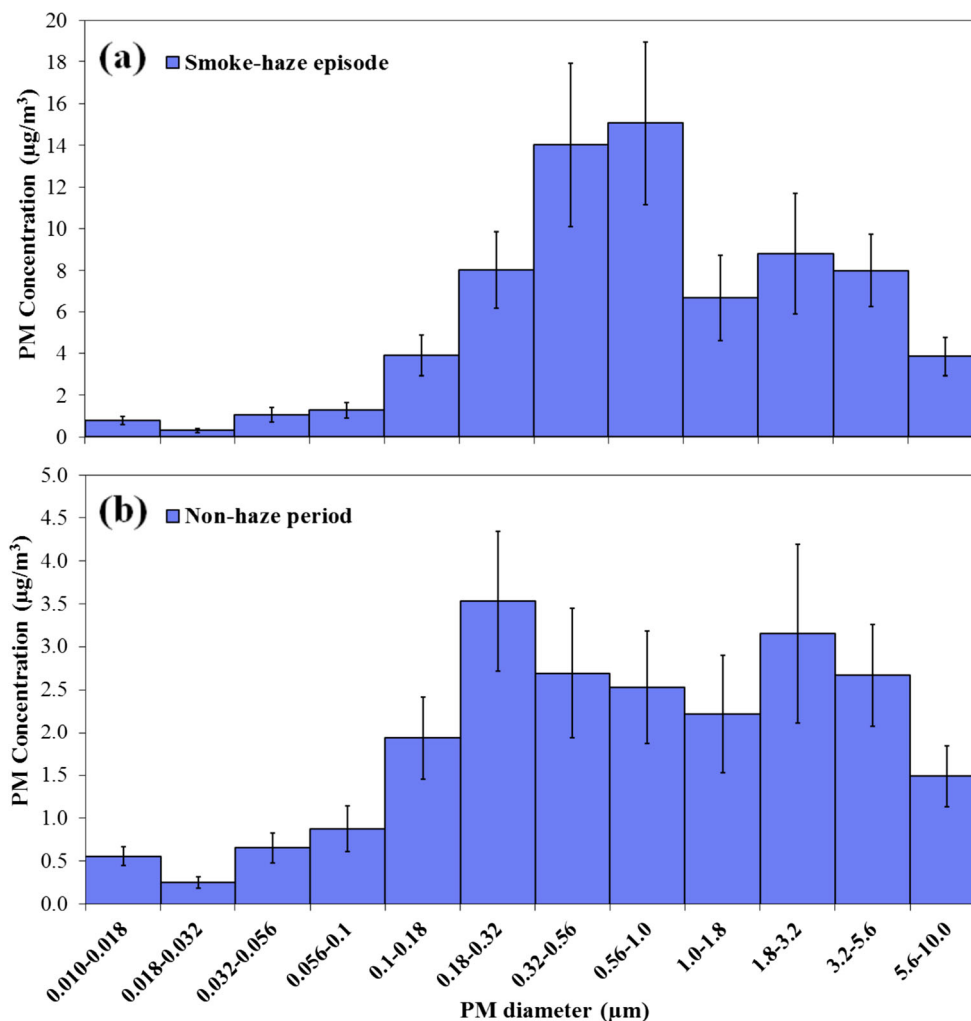
non-haze period, as can be seen from Fig. 3. For example, the ratios of concentration (smoke haze episode to non-haze period) of elements such as Co, Cr, Cd, Mn, and Sr were ≥5. Trace elements within the observed levels of elements present in fine particles during the smoke haze episode were classified into three groups: (i) major elements: Na, Fe, Al, Mg, K, Ca, B, Ba, Zn, and Ni ≥200 ng/m^3; (ii) sub-major elements: Se, Cu, Cr, Mn, and Pb ~30 to 199 ng/m^3; and (iii) minor elements: Sr, Co, Ga, Li, Tl, Te, Cd, Bi, and Be ≤30 ng/m^3. We used the same classification for trace elements measured during the non-haze period for consistency. Figure 3(a1), (a2) show the levels of major elements in coarse, fine, ultrafine, and nano particles during the two distinct periods. The mean concentrations of major elements in coarse, fine, ultrafine, and nano particles were 2158, 5211, 760, and 470 ng/m^3 during the smoke haze episode and 1109, 2166, 295, and 179 ng/m^3 during the non-haze period, respectively.

Most of the major elements (Na, Fe, Al, Mg, K, and Ca) are normally of crustal origin, while the remaining elements (B, Ba, Zn, and Ni) are derived from anthropogenic sources

(Duan et al. 2005; Lin et al. 2005; Duan et al. 2012). The presence of B, Ba, Zn, and Ni in the group of major elements suggested that the air quality at the measurement site was influenced by vehicular and industrial activities during the non-haze period. However, the increase in levels of major elements during the smoke haze episode confirmed that the trans-boundary transport from biomass burning emissions could have a significant impact on the atmospheric loading of particulate elements (Betha et al. 2013).

Figure 3(b1), (b2) show the levels of sub-major elements in coarse, fine, ultrafine, and nano particles during the two distinct periods. The corresponding mean concentrations of sub-major elements (Se, Cu, Cr, Mn, and Pb) were 124, 512, 90, and 37 ng/m^3 during the smoke haze episode and 58, 217, 29, and 15 ng/m^3 during the non-haze period, respectively. Figure 3(c1), (c2) show the levels of minor elements (Sr, Co, Ga, Li, Tl, Te, Cd, Bi, and Be) in coarse, fine, ultrafine, and nano particles, during the two distinct periods. The corresponding mean concentrations of minor elements
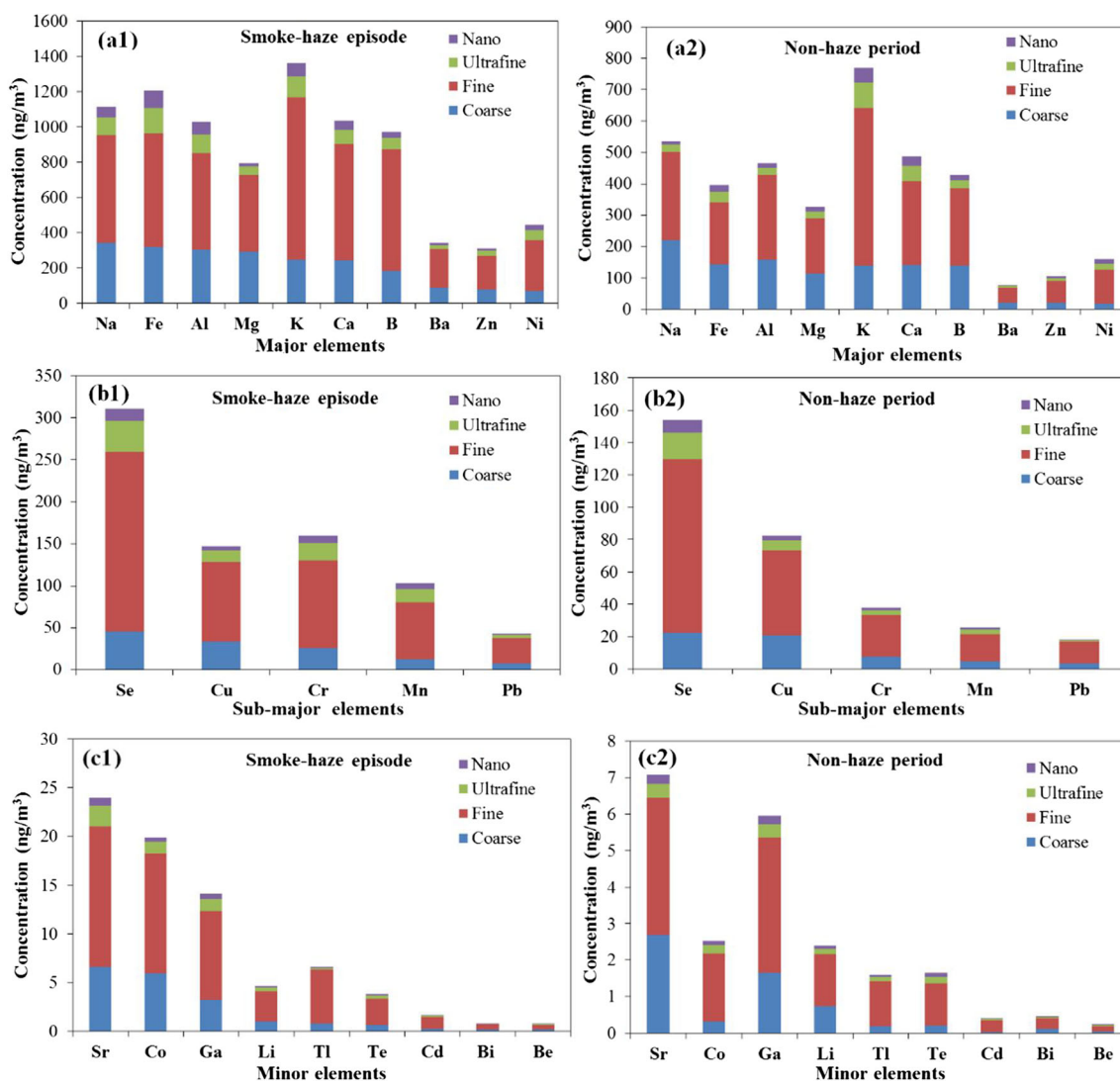
Fig. 3 Mass distribution of elemental composition in different size ranges of coarse, fine, ultrafine, and nano particles: major elements in the (**a1**) smoke haze period and (**a2**) non-haze period, sub-major elements in the (**b1**) smoke haze period and (**b2**) non-haze period, and minor elements in the (**c1**) smoke haze period and (**c2**) non-haze period

were 19, 50, 6, and 2 ng/m^3 during the smoke haze episode and 6, 14, 2, and 1 ng/m^3 during the non-haze period, respectively. From all four modes of particles, it is obvious that the major elements accounted for over 90 % of the total mass of the particulate elements in PM.

In addition to the above observations, it was clear that the patterns of elemental concentrations in different size distributions could fall into one of three distinct regions (region 1, region 2, and region 3). In region 1, elements are mostly concentrated in the coarse mode that includes Al, Ba, Ca, Fe, Mg, and Sr. The elements in region 2 are mostly concentrated in the accumulation mode, including Cd, Ni, Pb, Se, Te, and Tl. The remaining elements (B, Be, Bi, Co, Cr, Cu, Ga, K, Li, Mn, Na, and Zn) are considered under region 3, which showed multimode size distributions.

Source attribution for particulate-bound elements

To identify the enrichment of particulate elements either from crustal or anthropogenic origin, enrichment factors (EFs) of various elements were estimated using Eq. (2) as

$$EF_x = \frac{(C_x/Al)\text{aerosol}}{(C_x/Al)\text{crust}} \tag{5}$$

where "(C_x/Al)aerosol" represents the concentration ratio of element x (C_x) (in aerosol) to Al in aerosols, and "(C_x/Al)crust" represents the corresponding element (C_x)-to-Al ratio in crustal matter (Balasubramanian and Qian 2004; Behera and Sharma 2010).

In general, an element of purely crustal origin has a value of EF as 1. However, due to variations in crustal composition and uncertainties in fractionation during weathering, the EFs of elements of crustal origin may deviate from the specified magnitude, i.e., $1 < EF < 10$. Elements with $EF > 10$ are enriched, and a significant proportion of them has a non-crustal source (Marcazzan et al. 2001; Zhang et al. 2002). Elements with $EF < 10$ are non-enriched, and a significant proportion of them originates from crustal sources (Marcazzan et al. 2001; Zhang et al. 2002).

Figure 4 shows EFs of elements in coarse, fine, ultrafine, and nano particles during the smoke haze episode and the non-haze period. The estimated values of EFs during both the smoke haze and non-haze period were as follows: (1) 10–100 for Ba, Be, Co, Cr, Ga, and Li; (2) 100–1000 for Cd, Cu, Ni, Pb, Tl, and Zn; (3) 1000–10,000 for B and Bi; and (4) 100,000–1,000,000 for Se and Te. However, Ca, Fe, K, Mg, Mn, Na, and Sr have EFs<10 for all sizes of PM (except K, in the ultrafine and nano particles during the smoke haze episode), indicating that these elements were derived predominantly from crustal sources. However, K appears to be of mixed origin (from crustal and non-crustal sources). It should be noted that K is also considered to be an indicator of biomass burning, i.e., when biomass burning sources become dominant, the levels of K are also increased (See et al. 2006; Ye et al. 2011; Shon et al. 2012). The higher enrichment of ($EF > 10$) of K in ultrafine and nano particles during the smoke haze episode indicates the importance of biomass burning as an additional source of K. In addition, the statistical test, using the paired t test for both smoke haze and non-haze samples, revealed that there is a significant difference ($P < 0.05$) in the enrichment factors for K, Fe, Ni, Zn, and Cd between the smoke haze and non-haze periods. However, the remaining elements have no significant difference, with $P > 0.05$.
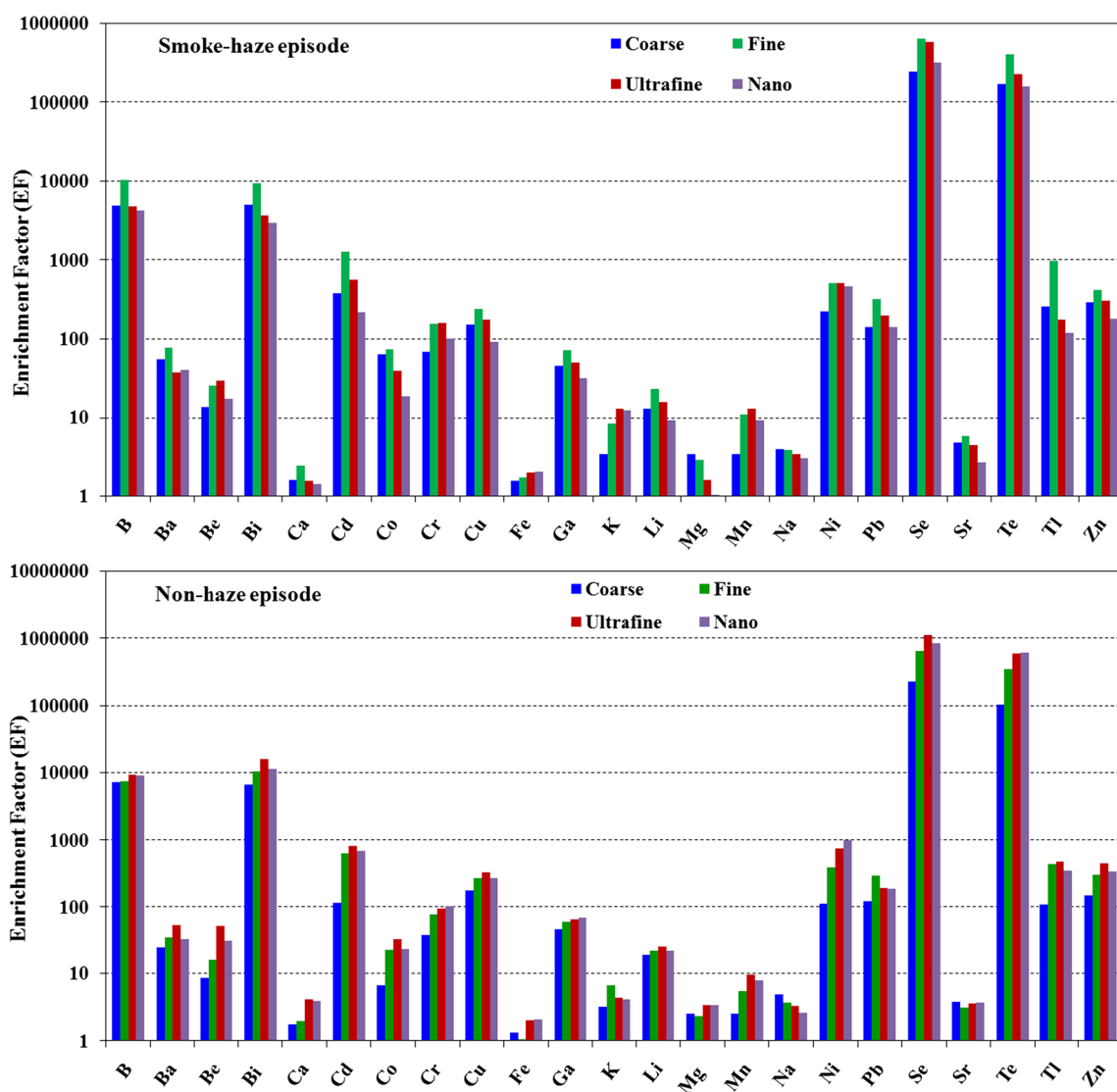

Fig. 4 Enrichment factors (EFs) of elements in coarse, fine, ultrafine, and nano particles during smoke haze episode and non-haze period

From the above facts, it was clear that Ba, Be, Co, Cr, Ga, Li, Cd, Cu, Ni, Pb, Tl, Zn, B, Bi, Se, and Te were enriched and derived from non-crustal sources. The non-crustal sources could be local anthropogenic sources, including vehicular emissions, industrial emissions, domestic cooking, etc., during the non-haze period. However, during the smoke haze episode, apart from the local anthropogenic sources, the trans-boundary transport from biomass burning emissions in Indonesia could also be responsible. To identify the role of trans-boundary emissions from biomass burning on the local air quality, PCA and backward trajectory analyses were performed during the smoke haze episode and the non-haze period.

The archived data of the Global Data Assimilation System of the National Oceanic and Atmospheric Administration (NOAA) was utilized in the Air Resource Laboratory (ARL) Hybrid Single-Particle Lagrangian Integrated Trajectory (HYSPLIT) model, to obtain the air mass back-trajectories (Draxler and Rolph 2013). The backward trajectory analysis was simulated at 14:00 hours (local time) at 500, 1000, and 1500 m above the ground level, for the duration of 120 h during the sampling period. Figure 5 presents the representative results of the backward trajectory analysis during the two distinctly different time periods. During the smoke haze episode, in terms of wind direction, the meteorology was favorable towards bringing the air masses from biomass fires (hotspots) taking place in Indonesia to Singapore. On the other hand, during the non-haze period, the wind direction was just the opposite of what was experienced during the smoke haze episode. Therefore, it appears that trans-boundary transport from biomass burning emissions intermixed with the local anthropogenic sources (vehicular, industrial, and domestic emissions) enhanced the concentrations of particulate elements during the smoke haze episode.

In this study, the data of particulate elemental concentrations were used in Minitab 15 English to perform PCA with varimax rotation, to extract the major sources of the trace elements. This method yielded a number of key factors associated with the chemical fingerprint elements of different sources. To obtain accurate results by PCA, it is essential that the data sets should contain an adequate number of PM samples. As reported by Henry et al. (1984), the number of samples to run (N) should be greater than $30+((V+3)/2)$, where V is the number of elements. With the number of elements being 24 in this study, the number of PM samples required to run the PCA for accurate results should be greater than 44. As we had four sampling days for the smoke haze episode and five for the non-haze period, we preferred the results of all size fractions in a single run of the data sets. In this process, the number of sample runs was 48 and 60, during the smoke haze episode and the non-haze period, respectively. We therefore performed the PCA separately for the non-haze period and the smoke haze episode. In both these sampling periods, elemental concentrations in all PM size ranges were considered as inputs in the PCA analysis. Tables 3 and 4 present the PCA factor loadings for all measured elements during the non-haze period and the smoke haze episode, respectively.

As shown in Table 3 for the non-haze period, the PCA identified four possible sources as factors, PC1, PC2, PC3, and PC4. The first factor (PC1) was heavily loaded with Al, Ca, Fe, Ga, K, Mg, Mn, Na, and Sr with a variance of 42.2 % and an eigenvalue of 11.7. These elements could likely be from nearby roads and/or crustal dust particles (Marcazzan et al. 2001; Trapp et al. 2010). In addition, K may originate from biomass burning-related sources in the form of fine soil particles, transported from hot spots by prevailing winds. PC2 was heavily loaded with Ba, Cd, Cu, Ni, Se, and Zn, with a variance of 24.5 % and an eigenvalue of 6.8. The overloaded elements in PC2 are normally associated with vehicular emission sources and therefore represent the influence of vehicular emissions (Marcazzan et al. 2001; Lin et al. 2005). PC3 was heavily loaded with B, Be, Bi, Co, Pb, Te, and Zn, with a variance of 16.9 % and an eigenvalue of 4.7. Out of all the elements identified in PC3, Be, Bi, B, Co, and Te were generally from industrial sources, while Pb and Zn were from waste incinerators (Marcazzan et al. 2001; Trapp et al. 2010; Lin et al. 2005). Therefore, it could be inferred that the overloading of elements in PC3 was mostly influenced by point sources of pollution. PC4 was overloaded with Cr with a variance of 12.3 % and an eigenvalue of 3.4. Cr is a well-known marker of PM emissions from power plants, industries, and fossil fuel combustion (Marcazzan et al. 2001; Lin et al. 2005). As the sampling site was not far from the industrial area, it appears that the Cr in PM was mainly derived from power plants and petrochemical plants.

For the smoke haze episode, the observation was slightly different from that during the non-haze period. As shown in Table 4, the fourth factor, PC4, had more elements with significant loadings compared to the non-haze period. The reason for such observations could be due to the trans-boundary transport of biomass burning emissions, intermixed with emissions from local anthropogenic sources during the smoke haze episode, which might increase the atmospheric loading of some trace elements. The previous study of Betha et al. (2013) also found significantly higher concentrations of Al, Cr, K, Ni, and Pb in emissions of Indonesia peat fires compared to background emissions. Therefore, it can be confirmed that the long-range transport of biomass burning emissions occurring in Indonesia contributed a significant proportion of particulate elements to the local air pollution in Singapore. Thus, the combined impact of local urban PM emissions and the long-range transport of biomass
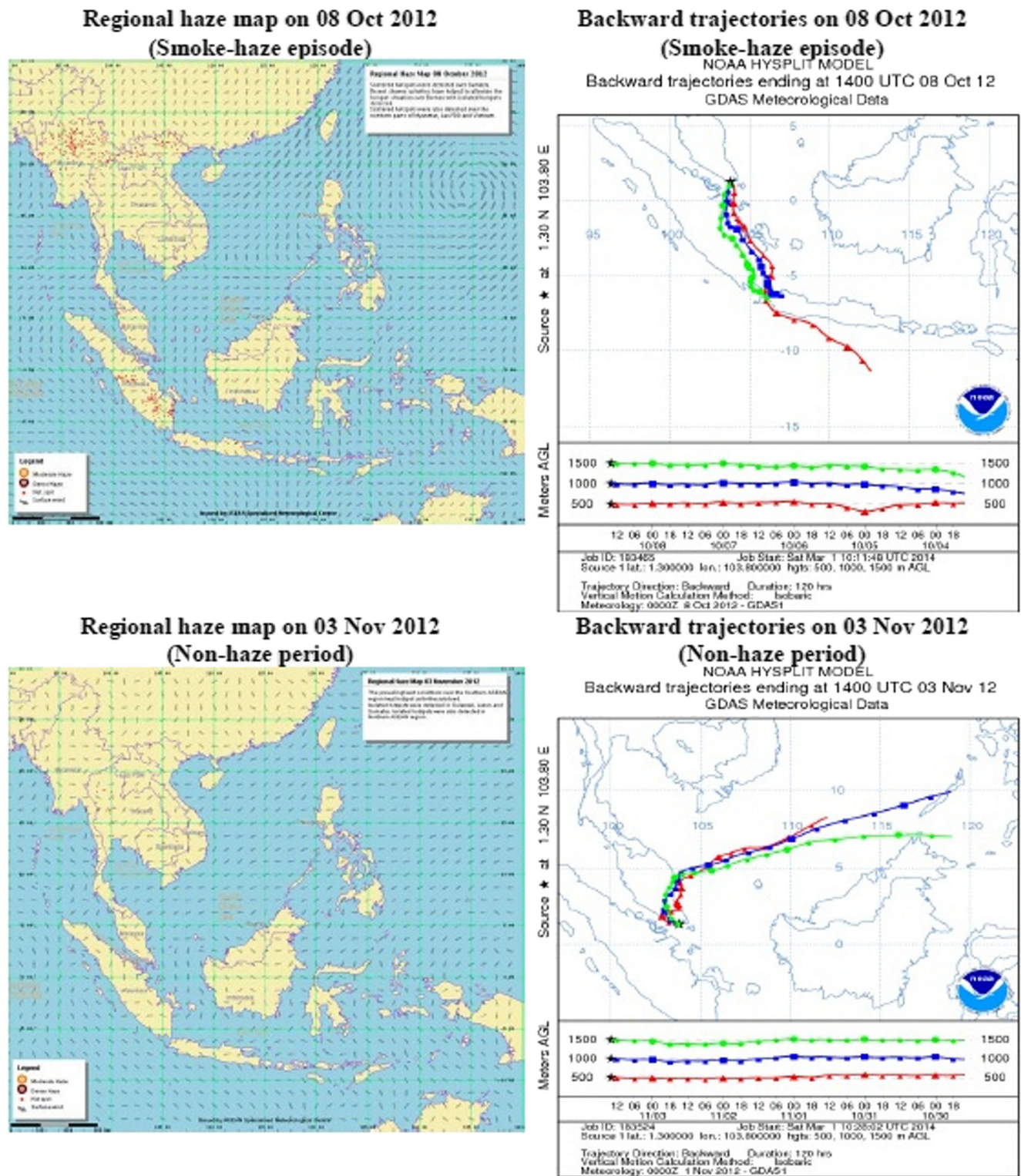
**Regional haze map on 08 Oct 2012
(Smoke-haze episode)**

**Backward trajectories on 08 Oct 2012
(Smoke-haze episode)**

**Regional haze map on 03 Nov 2012
(Non-haze period)**

**Backward trajectories on 03 Nov 2012
(Non-haze period)**

Fig. 5 Regional haze maps (source: NEA, Singapore) and backward trajectories from the outputs of HYSPLIT model (NOAA, USA) during the smoke haze episode and non-haze period

burning emissions might be the reason for the increased levels of particulate elements in four modes of PM (coarse, fine, ultrafine, and nano) during the smoke haze episode as shown in Fig. 3.

Particulate element deposition in the respiratory system

As explained in "Deposition modeling in the respiratory system", MPPD modeling was performed with adjusted specific

Table 3 PCA factor loadings for particulate elements during non-haze period

Elements	Factors			
	PC1	PC2	PC3	PC4
Al	0.96			
B			0.94	
Ba		0.94		
Be			0.82	
Bi		0.53	0.84	
Ca	0.97			
Cd		0.96		0.52
Co			0.94	
Cr				0.92
Cu		0.82		
Fe	0.94			
Ga	0.91			
K	0.96			
Li	0.53			
Mg	0.97			
Mn	0.94			
Na	0.92			
Ni		0.96		
Pb			0.95	
Se		0.91		
Sr	0.92			
Te			0.91	
Tl		0.64		
Zn		0.92	0.61	
Eigenvalue	11.7	6.8	4.7	3.4
Variance (%)	42.4	24.5	16.9	12.3
Cumulative %	42.4	66.9	83.8	96.1

Extraction method: principal component analysis; rotation method: varimax; only factor loadings ≥0.5 listed; only factors with eigenvalue ≥1 shown; source apportionment method: PCA

Table 4 PCA factor loadings for particulate elements during smoke haze episode

Elements	Factors			
	PC1	PC2	PC3	PC4
Al	0.82			0.68
B			0.81	0.59
Ba		0.92		
Be			0.78	0.91
Bi		0.58	0.81	
Ca	0.94			
Cd		0.96	0.53	
Co			0.84	0.62
Cr				0.96
Cu		0.86	0.52	
Fe	0.86			0.52
Ga	0.92			
K	0.76			0.61
Li	0.56			
Mg	0.92			
Mn	0.86			0.69
Na	0.94			
Ni		0.89		0.51
Pb			0.76	0.54
Se		0.82		0.68
Sr	0.92			
Te			0.71	
Tl		0.84		
Zn		0.72	0.64	
Eigen value	10.1	6.2	4.3	3.5
Variance (%)	39.8	23.4	15.7	12.9
Cumulative %	39.8	63.2	78.9	91.8

Extraction method: principal component analysis; rotation method: varimax; only factor loadings≥0.5 listed; only factors with eigenvalue ≥1 shown; source apportionment method: PCA

model parameters to estimate deposition fractions of different sizes of PM mass and their corresponding elemental composition. Figure 6 shows the average deposition fractions of coarse, fine, ultrafine, and nano particles in the head, tracheobronchial, and pulmonary regions of the human respiratory system during the non-haze period and the smoke haze episode. Among all the sizes, coarse particles had the highest deposition fractions in the head region of the respiratory system (non-haze, 39 %; smoke haze, 34 %) followed by fine particles (non-haze, 25 %; smoke haze, 22 %). The deposition of larger fractions of coarse and fine particles on the head airways could be due to a combination of sedimentation and the impaction of particles onto the larynx and airway bifurcations (Zhang and Yu 1993).

The deposition patterns of ultrafine and nano particles were observed to be different from those of coarse and fine particles with regard to greater deposition of those particles occurred in the pulmonary region, in comparison to other regions of the respiratory system. The deposition fractions in the pulmonary region during the non-haze period and the smoke haze episode were as follows: coarse, 19 and 21 %; fine, 15 and 21 %; ultrafine, 21 and 25 %, nano, 25 and 28 %; respectively. This deposition pattern could be due to the fact that the flow path of smaller particles in the human respiratory system is primarily governed by Brownian diffusion, leading to their preferential deposition in the pulmonary region (Ingham 1984; Martins et al. 2010; Ham et al. 2011).

This study finds that the particle depositions in the respiratory system would be more severe during the smoke haze episode than during the non-haze period. In addition, the average deposition fractions of fine, ultrafine, and nano particles in the
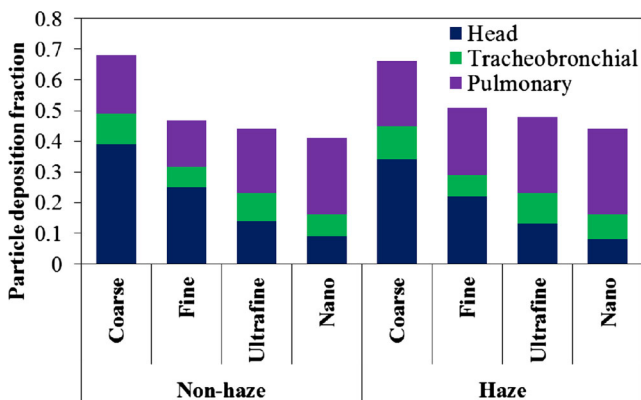
Fig. 6 Deposition fractions of coarse, fine, ultrafine, and nano particles in pulmonary, tracheobronchial, and head regions of the human body

tracheobronchial and pulmonary regions increased during the smoke haze episode, while they decreased in the head airway region. The reason for such observations could be due to accumulation of submicron-sized particles in the accumulation mode during the smoke haze episode, as discussed in the previous section. In addition, higher particle mass or number concentrations during the smoke haze episode could also increase the probability of particle deposition

in the respiratory system. Overall, it was confirmed that more deposits of finer particles can reach the innermost region of the human respiratory system, in comparison to coarse particles. Therefore, prolonged exposure to lower concentrations of ultrafine and nano particles present in the ambient air can cause adverse health impacts.

Figure 7 shows the mean deposition efficiencies of all elements of fine particles in the head, tracheobronchial, and pulmonary regions, in the units of microgram of each component deposited per microgram fine particle component mass inhaled. The outputs of the MPPD modeling were used to estimate the individual deposition efficiency during the smoke haze episode and the non-haze period, as explained in "Deposition modeling in the respiratory system". Only the fine particles ($PM_{2.5}$) were considered, since they represent a commonly regulated air pollutant and included as a part of the national ambient air quality standards in many countries. The total deposition efficiency (the sum of head, tracheobronchial, and pulmonary regions) varied from 41 % (B) to 55 % (Mg) for various elements during the smoke haze episode and 35 % (Cu) to 53 % (Ca) during the non-haze period. The head region had a higher deposition of the elements that were more concentrated in the coarse mode. Pb had the lowest amount deposited in the head region: 15 and 17 %

Fig. 7 Mean deposition efficiencies various elements of fine particles in all of the respiratory regions during the **(a)** haze episode and **(b)** non-haze period (head, tracheobronchial, and pulmonary) (units: μg of each component deposited per μg fine particle component mass inhaled)
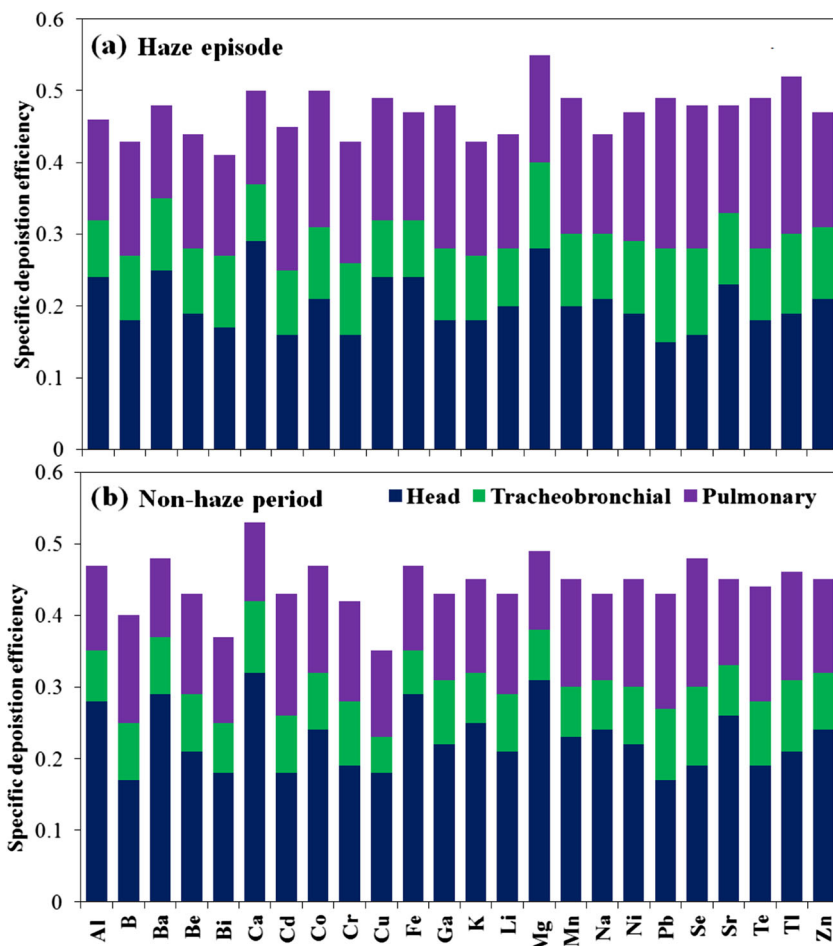
during the smoke haze episode and the non-haze period, respectively. The highest deposition in the head region was observed for Ca, at 29 and 32 % during the smoke haze episode and the non-haze period, respectively.

Similar to the observations on deposition in the pulmonary region, trace elements also exhibited trends of higher deposition in the tracheobronchial region during the smoke haze episode, compared to during the non-haze period. Overall, it was observed that the trace elements that are concentrated in the accumulation mode have a higher probability of getting deposited in the innermost region of the human respiratory system.

Summary and conclusions

The present study investigated the size-resolved characterization of 24 trace elements present in atmospheric PM during a recent smoke haze episode that occurred in Singapore. The results of elemental characterization were used in HYSPLIT and PCA models, to assess the influence of the smoke haze episode on the increased atmospheric loading of particulate-bound elements. For assessment of the potential health impacts on humans, the MPPD model was used to estimate the particle deposition fractions of three regions (head, tracheobronchial, and pulmonary) of the human respiratory system. The results of elemental characterization showed that (i) the elements concentrated in the coarse mode were Al, Ba, Ca, Fe, Mg, and Sr; (ii) the elements concentrated in the accumulation mode were Cd, Ni, Pb, Se, Te, and Tl; and (iii) the remaining elements (B, Be, Bi, Co, Cr, Cu, Ga, K, Li, Mn, Na, and Zn) showed multimode distributions. The ratios of the concentration of elements during the smoke haze episode and non-haze period in coarse, fine, ultrafine, and nano particles varied in the range from 1.4 (Li) to 6.3 (Cd), 2.0 (Bi) to 6.6 (Co), 1.2 (Bi) to 5.7 (Mn), and 1.2 (Bi) to 5.5 (Mn). The estimated EFs confirmed that Ba, Be, Co, Cr, Ga, Li, Cd, Cu, Ni, Pb, Tl, Zn, B, Bi, Se, and Te were enriched in the atmosphere, due to emissions from non-crustal sources. The backward trajectory analysis of air masses based on HYSPLIT modeling showed that the prevailing wind direction during the smoke haze episode brought biomass burning-impacted air masses to Singapore from Indonesia. The PCA revealed that the trans-boundary transport of biomass burning emissions was primarily responsible for the enhanced concentration of particulate elements during the smoke haze episode. The MPPD modeling results revealed that coarse particles had the highest deposition fractions in the head region of the respiratory system (smoke haze, 34 %; non-haze, 39 %) followed by fine particles (smoke haze, 22 %; non-haze, 25 %). For ultrafine and nano particles, the deposition fractions were higher in the pulmonary region than in the head region. This study suggests that prolonged exposure to lower concentrations of ultrafine and nano particles present in the atmosphere raises health concerns.

References

Abas MRB, Rahman NA, Omar NYMJ, Maah MJ, Samah AA, Oros DR, Otto A, Simoneit BRT (2004) Organic composition of aerosol particulate matter during a haze episode in Kuala Lumpur, Malaysia. Atmos Environ 38(25):4223–4241

Alfoldy B, Giechaskiel B, Hofmann W, Drossinos Y (2009) Size-distribution dependent lung deposition of diesel exhaust particles. J Aerosol Sci 40(8):652–663

Anjilvel S, Asgharian B (1995) A multi-path model of particle deposition in the rat lung. Fundam Appl Toxicol 58:41–50

Asgharian B, Anjilvel S (1998) A multiple-path model of fiber deposition in the rat lung. Toxicol Sci 44(1):80–86

Asgharian B, Price OT (2007) Deposition of ultrafine (nano) particles in the human lung. Inhal Toxicol 19:1045–1052

Balasubramanian R, Qian WB (2004) Characterization and source identification of airborne trace metals in Singapore. J Environ Monit 6(10):813–818

Balasubramanian R, Victor T, Begum R (1999) Impact of biomass burning on rainwater acidity and composition in Singapore. J Geophys Res 104(D21):26881–26890

Balasubramanian R, Qian WB, Decesari S, Facchini MC, Fuzzi S (2003) Comprehensive characterization of PM$_{2.5}$ aerosols in Singapore. J Geophys Res 108:4523

Behera SN, Balasubramanian R (2014). Influence of biomass burning on temporal and diurnal variations of acidic gases, particulate nitrate, and sulfate in a tropical urban atmosphere. Advances in Meteorology, Article ID 828491, doi:10.1155/2014/828491

Behera SN, Sharma M (2010) Reconstructing primary and secondary components of PM$_{2.5}$ composition for an urban atmosphere. Aerosol Sci Technol 44(11):983–992

Behera SN, Betha R, Liu P, Balasubramanian R (2013) A study of diurnal variations of PM$_{2.5}$ acidity and related chemical species using a new thermodynamic equilibrium model. Sci Total Environ 452:286–295

Betha R, Pradani M, Lestari P, Joshi UM, Reid JS, Balasubramanian R (2013) Chemical speciation of trace metals emitted from Indonesian peat fires for health risk assessment. Atmos Res 122:571–578

Betha R, Behera SN, Balasubramanian R (2014) 2013 Southeast Asian smoke haze: fractionation of particulate-bound elements and associated health risk. Environ Sci Technol 48(8):4327–4335

Carmine PD, Lucarelli F, Mando PA, Valerio M, Prati P, Zucchiatti A (1999) Elemental composition of size-fractionated urban aerosol collected in Florence, Italy; preliminary results. Nucl Instrum Methods Phys Res B 150:450–456

Carter JD, Ghio AJ, Samet JM, Devlin RB (1997) Cytokine production by human airway epithelial cells after exposure to an air pollution particle is metal-dependent. Toxicol Appl Pharm 146(2):180–188

Clements N, Eav J, Xie M, Hannigan MP, Miller SL, Navidi W, Jennifer LP, Schauer JJ, Shafer MM, Milford JB (2014) Concentrations and source insights for trace elements in fine and coarse particulate matter. Atmos Environ 89:373–381

Dillner AM, Shafer MM, Schauer JJ (2007) A novel method using polyurethane foam (PUF) substrates to determine trace element concentrations in size-segregated atmospheric particulate matter on short time scales. Aerosol Sci Technol 41(1):75–85

Draxler RR, Rolph GD (2013). HYSPLIT (HYbrid Single-Particle Lagrangian Integrated Trajectory) Model access via NOAA ARL

READY Website (http://www.arl.noaa.gov/HYSPLIT.php). NOAA Air Resources Laboratory, College Park, MD

Duan JC, Bi XH, Tan JH, Sheng GY, Fu JM (2005) The differences of the size distribution of polycyclic aromatic hydrocarbons (PAHs) between urban and rural sites of Guangzhou, China. Atmos Res 78(3): 190–203

Duan JC, Bi XH, Tan JH, Sheng GY, Fu JM (2006) The particle diameter distribution of polycyclic aromatic hydrocarbons (PAHs) in atmospheric particle during haze, China. Environ Sci 26(1):6–10 (in Chinese)

Duan J, Tan J, Wang S, Hao J, Chai F (2012) Size distributions and sources of elements in particulate matter at curbside, urban and rural sites in Beijing. J Environ Sci 24(1):87–94

Elder A, Oberdorster G (2006) Translocation and effects of ultrafine particles outside of the lung. Clin Occup Environ Med 5:785–796

U.S. Environmental Protection Agency, USEPA (1991). Determination of trace elements in waters and wastes by inductively coupled plasma-mass spectrometry, revision 4.4, EPA-600-R-94-111, April 1991

Fang GC, Wu YS, Wen CC, Lin CK, Huang SH, Rau JY, Lin CP (2005) Concentrations of nano and related ambient air pollutants at a traffic sampling site. Toxicol Ind Health 21(9):259–271

Farina F, Sancini G, Battaglia C, Tinaglia V, Mantecca P, Camatini M, Palestini P (2013) Milano summer particulate matter (PM$_{10}$) triggers lung inflammation and extra pulmonary adverse events in mice. PLoS One 8(2):e56636

Ghio AJ, Stonehuerner J, Dailey LA, Carter JD (1999) Metals associated with both the water-soluble and insoluble fractions of an ambient air pollution particle catalyze an oxidative stress. Inhal Toxicol 11(1):37–49

Ham WA, Herner JD, Green PG, Kleeman MJ (2010) Size distribution of health-relevant trace elements in airborne particulate matter during a severe winter stagnation event: implications for epidemiology and inhalation exposure studies. Aerosol Sci Technol 44(9):753–765

Ham WA, Ruehl CR, Kleeman MJ (2011) Seasonal variation of airborne particle deposition efficiency in the human respiratory system. Aerosol Sci Technol 45(7):795–804

Heil A, Goldammer J (2001) Smoke-haze pollution: a review of the 1997 episode in Southeast Asia. Reg Environ Change 2(1):24–37

Henry RC, Hidy GM (1979) Multivariate analysis of particulate sulfate and other air quality variables by principal components—part 1. Annual data from Los Angeles and New York. Atmos Environ 13(11):1581–1596

Henry RC, Lewis CW, Hopke PK, Williamson HJ (1984) Review of receptor model fundamentals. Atmos Environ 18(8):1507–1515

Herner JD, Green PG, Kleeman MJ (2006) Measuring the trace elemental composition of size-resolved airborne particles. Environ Sci Technol 40(6):1925–1933

Homazava N, Ulrich A, Krähenbühl U (2008) Spatially and time-resolved element-specific in situ corrosion investigations with an online hyphenated microcapillary flow injection inductively coupled plasma mass spectrometry set-up. Spectrochim Acta B 63(7):777–783

Hyer EJ, Chew BN (2010) Aerosol transport model evaluation of an extreme smoke episode in Southeast Asia. Atmos Environ 44(11): 1422–1427

Ingham DB (1984) Diffusion of aerosols from a stream flowing through a short cylindrical pipe. J Aerosol Sci 15(5):637–641

Kabir E, Kim KH, Yoon HO (2011) Trace metal contents in barbeque (BBQ) charcoal products. J Hazard Mater 185(2):1418–1424

Kane DB, Asgharian B, Price OT, Rostami A, Oldham MJ (2010) Effect of smoking parameters on the particle size distribution and predicted airway deposition of mainstream cigarette smoke. Inhal Toxicol 22(3):199–209

Karar K, Gupta AK (2007) Source apportionment of PM$_{10}$ at residential and industrial sites of an urban region of Kolkata, India. Atmos Res 84(1):30–41

Karthikeyan S, Joshi UM, Balasubramanian R (2006) Microwave assisted sample preparation for determining water-soluble fraction

of trace elements in urban airborne particulate matter: evaluation of bioavailability. Anal Chim Acta 576(1):23–30

Khare P, Baruah BP (2010) Elemental characterization and source identification of PM$_{2.5}$ using multivariate analysis at the suburban site of North-East India. Atmos Res 98(1):148–162

Kim YH, Kim KH (2012) Ultimate detectability of volatile organic compounds: how much further can we reduce their ambient air sample volumes for analysis? Anal Chem 84(19):8284–8293

Kim KH, Choi GH, Kang CH, Lee JH, Kim JY, Youn YH, Lee SR (2003) The chemical composition of fine and coarse particles in relation with the Asian Dust events. Atmos Environ 37(6):753–765

Kothai P, Saradhi IV, Pandit GG, Markwitz A, Puranik VD (2011) Chemical characterization and source identification of particulate matter at an urban site of Navi Mumbai, India. Aerosol Air Qual Res 11:560–569

Koulouri E, Saarikoski S, Theodosi C, Markaki Z, Gerasopoulos E, Kouvarakis G, Ma¨kela¨ T, Hillamo R, Mihalopoulos N (2008) Chemical composition and sources of fine and coarse aerosol particles in the Eastern Mediterranean. Atmos Environ 42(26):6542–6550

Lai CH, Chen KS, Wang HK (2009) Influence of rice straw burning on the levels of polycyclic aromatic hydrocarbons in agricultural county of Taiwan. J Environ Sci 21(9):1200–1207

Leiva GMA, Santibañez DA, Ibarra ES, Matus CP, Seguel R (2013) A five-year study of particulate matter (PM$_{2.5}$) and cerebrovascular diseases. Environ Pollut 181:1–6

Lin CC, Chen SJ, Huang KL, Hwang WI, Chang-Chien GP, Lin WY (2005) Characteristics of metals in nano/ultrafine/fine/coarse particles collected beside a heavily trafficked road. Environ Sci Technol 39(21):8113–8122

Marcazzan GM, Vaccaro S, Valli G, Vecchi R (2001) Characterization of PM$_{10}$ and PM$_{2.5}$ particulate matter in the ambient air of Milan, Italy. Atmos Environ 35:4639–4650

Martins LD, Martins JA, Freitas ED, Mazzoli CR, Gonçalves FLT, Ynoue RY, Hallak R, Albuquerque TTA, de Fatima AM (2010) Potential health impact of ultrafine particles under clean and polluted urban atmospheric conditions: a model-based study. Air Qual Atmos Health 3(1):29–39

Menon S, Hansen J, Nazarenko L, Luo Y (2002) Climate effects of black carbon aerosols in China and India. Science 297(5590):2250–2253

Mura¨nszky G, O¨va¨ri M, Vira¨g I, Csiba P, Dobai R, Za¨ray G (2011) Chemical characterization of PM$_{10}$ fractions of urban aerosol. Microchem J 98(1):1–10

Nazaroff WW, Hung WY, Sasse AGBM, Gadgil AJ (1993) Predicting regional lung deposition of environmental tobacco-smoke particles. Aerosol Sci Technol 19(3):243–254

Nel A (2005) Air pollution-related illness: effects of particles. Science 308(5723):804–806

Nong A, Taylor MD, Clewell HJ, Dorman DC, Andersen ME (2009) Manganese tissue dosimetry in rats and monkeys: accounting for dietary and inhaled Mn with physiologically based pharmacokinetic modeling. Toxicol Sci 108:22–34

O'Shaughnessy PT, Raabe OG (2003) A comparison of cascade impactor data reduction methods. Aerosol Sci Technol 37(2):187–200

Oberdorster G, Sharp Z, Atudorei V, Elder A, Gelein R, KreylingW CC (2004) Translocation of inhaled ultrafine particles to the brain. Inhal Toxicol 16:437–445

Pavagadhi S, Betha R, Venkatesan S, Balasubramanian R, Hande MP (2013) Physicochemical and toxicological characteristics of urban aerosols during a recent Indonesian biomass burning episode. Environ Sci Pollut Res Int 20(4):2569–2578

Reid JS, Hyer EJ, Johnson RS, Holben BN, Yokelson RJ, Zhang J, Campbell JR, Christopher SA, Girolamo LD, Giglio L, Holz RE, Kearney C, Miettinen J, Reid EA, Turk FJ, Wang J, Xian P, Zhao G, Balasubramanian R, Chew BN, Janjai S, Lagrosas N, Lestari P, Lin N-H, Mahmud M, Nguyen AX, Norris B, Oanh NTK, Oo M, Salinas SV, Welton EJ, Liew SC (2013) Observing and

understanding the Southeast Asian aerosol system by remote sensing: an initial review and analysis for the Seven Southeast Asian Studies (7SEAS) program. Atmos Res 122:403–468

Rostami AA (2009) Computational modeling of aerosol deposition in respiratory tract: a review. Inhal Toxicol 21(4):262–290

Russell AG, Brunekreef B (2009) A focus on particulate matter and health. Environ Sci Technol 43(13):4620–4625

Salvador P, Artinano B, Alonso DG, Querol X, Alastuey A (2004) Identification and characterization of sources of PM_{10} in Madrid (Spain) by statistical methods. Atmos Environ 38(3):435–447

See SW, Balasubramanian R, Wang W (2006) A study of the physical, chemical, and optical properties of ambient aerosol particles in Southeast Asia during hazy and nonhazy days. J Geophys Res 111:D10S08. doi:10.1029/2005JD006180

See SW, Balasubramanian R, Rianawati E, Karthikeyan S, Streets DG (2007) Characterization and source apportionment of particulate matter≤2.5 μm in Sumatra, Indonesia, during a recent peat fire episode. Environ Sci Technol 41(10):3488–3494

Shon ZH, Kim KH, Song SK, Jung K, Kim NJ, Lee JB (2012) Relationship between water-soluble ions in $PM_{2.5}$ and their precursor gases in Seoul megacity. Atmos Environ 59:540–550

Sioutas C, Delfino RJ, Manisha S (2005) Exposure assessment for atmospheric ultrafine particles (UFPs) and implications in epidemiologic research. Environ Health Perspect 113:947–955

Szoke R, Alfoldy B, Balashazy I, Hofmann W, Sziklai-Laszlo I (2007) Size distribution, pulmonary deposition and chemical composition of Hungarian biosoluble glass fibers. Inhal Toxicol 19(4):325–332

Tan JH, Duan JC, Chen DH, Wang XH, Guo SJ, Bi XH, Sheng G-Y, He K-B, Fu JM (2009) Chemical characteristics of haze during summer and winter in Guangzhou. Atmos Res 94(2):238–245

Teeguarden JG, Hinderliter PM, Orr G, Thrall BD, Pounds JG (2007) Particokinetics in vitro: dosimetry considerations for in vitro nano-particle toxicity assessments. Toxicol Sci 95(2):300–312

Thurston GD, Spengler JD (1985) A quantitative assessment of source contributions to inhalable particulate matter pollution in metropolitan Boston. Atmos Environ 19(1):9–25

Trapp JM, Millero FJ, Prospero JM (2010) Trends in the solubility of iron in dust-dominated aerosols in the equatorial Atlantic trade winds: importance of iron speciation and sources. Geochem Geophys Geosyst 11(3). doi:10.1029/2009GC002651

Vallius M, Russkanen J, Pekkanen J (2008) Comparison of multivariate source apportionment of urban PM 2.5 with chemical mass closure. Boreal Environ Res 13:347–358

Venkataraman C, Raymond J (1998) Estimating the lung deposition of particulate polycyclic aromatic hydrocarbons associated with multi-modal urban aerosols. Inhal Toxicol 10(3):183–204

Venkataraman C, Thomas S, Kulkarni P (1999) Size distributions of polycyclic aromatic hydrocarbons gas/particle partitioning to urban aerosols. J Arosol Sci 30(6):759–770

Wilson MR, Lightbody JH, Donaldson K, Sales J, Stone V (2002) Interactions between ultrafine particles and transition metals in vivo and in vitro. Toxicol Appl Pharm 184(3):172–179

Winter-Sorkina, R. de, and Cassee, F. R. 2002. From concentration to dose: factors influencing airborne particulate matter deposition in humans and rats. National Institute of Public Health and the Environment (RIVM), the Netherlands. Report 650010031/2002. http://www.rivm.nl/bibliotheek/rapporten/650010031.pdf

Yang HH, Tsai CH, Chao MR, Su YL, Chien SM (2006) Source identification and size distribution of atmospheric polycyclic aromatic hydrocarbons during rice straw burning period. Atmos Environ 40(7):1266–1274

Ye X, Ma Z, Zhang J, Du H, Chen J, Chen H, Yang X, Gao W, Geng F (2011) Important role of ammonia on haze formation in Shanghai. Environ Res Lett 6(2):024019

Zhang L, Yu CP (1993) Empirical equations for nasal deposition of inhaled particles in small laboratory—animals and humans. Aerosol SciTechnol 19(1):51–56

Zhang J, Wu Y, Liu CL, Shen ZB, Zhang Y (2002) Major components of aerosols in north China: desert region and the Yellow Sea in the spring and summer of 1995 and 1996. J Atmos Sci 59:1515–1532

Zhang W, Zhuang G, Guo J, Xu D, Wang W, Baumgardner D, Wu Z, Yang W (2010) Sources of aerosol as determined from elemental composition and size distributions in Beijing. Atmos Res 95(2):197–209